Computer Physics Communications 181 (2010) 473–480

Contents lists available at ScienceDirect

Computer Physics Communications

www.elsevier.com/locate/cpc

Momentum–time flux conservation method for one-dimensional wave equations

Zhen-Ting Huang [a], Huan-Chun Hsu [b], Chau-Lyan Chang [c], Chin-Tien Wu [a], T.F. Jiang [b,d,*]

[a] Institute of Mathematical Modeling and Scientific Computing, National Chiao-Tung University, Hsinchu 30010, Taiwan
[b] Institute of Physics, National Chiao-Tung University, Hsinchu 30010, Taiwan
[c] Computational Aerosciences Branch, NASA Langley Research Center, Hampton, VA 23681-2199, USA
[d] Center for Quantum Science and Engineering, National Taiwan University, Taipei 10617, Taiwan

ARTICLE INFO

Article history:
Received 24 March 2009
Received in revised form 21 September 2009
Accepted 19 October 2009
Available online 27 October 2009

ABSTRACT

We present a conservation element and solution element method in time and momentum space. Several paradigmatic wave problems including simple wave equation, convection–diffusion equation, driven harmonic oscillating charge and nonlinear Korteweg–de Vries (KdV) equation are solved with this method and calibrated with known solutions to demonstrate its use. With this method, time marching scheme is explicit, and the nonreflecting boundary condition is automatically fulfilled. Compared to other solution methods in coordinate space, this method preserves the complete information of the wave during time evolution which is an useful feature especially for scattering problems.

1. Introduction

In the early 90's, Chang et al. first introduced the idea of space–time flux conservation to solving the general wave problems [1], later coined the *conservation element and solution element* (CESE) method. Since its inception, the CESE method has shown distinguished power in solving wave equations in various fields, notable examples including problems in computational fluid dynamics, aeroacoustics, electromagnetism and magnetohydrodynamics, etc. [2]. In the CESE method, the *space* degree and the *time* degree of freedom are treated in an unified way. The space–time domain is discretized into solution elements (SE), and the nonoverlap space–time cells bounded by SE are called the conservation elements (CE), as depicted in Fig. 1. In each CE, the space–time flux conservation law is enforced, from which the time marching scheme is derived. The nonreflecting boundary condition (NRBC) [3] is naturally implied by applying the flux conservation idea at the boundary CE, requires no filter function, absorbing potential, etc. [4] near the boundary to keep the numerical region from being contaminated by the aliased reflection at the numerical boundary.

However, there is a general problem in coordinate space calculations: the correct information is obtained in the model numerical region, but the part of wave outside of the numerical region which is of interest in some physics problems, is lost. For example, in the problem of highly excited states or the photoionized electron spectrum, the wave function extends to a very large spatial range, making calculations in coordinate space intractable. Theoretically, the coordinate space and the momentum space representations are equivalent and complementary to each other in case the solution is complete. This complementarity implies that a widely diffusive wave in coordinate space will correspond to a narrowly localized one in momentum space, and because momentum is directly related to kinetic energy, extremely large momentum for a system would usually be unphysical. Thus a moderate momentum region will be sufficient for a numerical modeling of complete information. Also, the wave will simply vanish at the numerical boundary and cause no trouble like methods in coordinate space. Naturally, solving problems in momentum space was attempted, yet difficulties such as singularity in Coulombic system are usually encountered [5]. Some method such as Lande regularization was proposed to resolve that singularity, but the range of momentum space must be unreasonably large to produce correct eigenstates, causing a disadvantage in practice. Recently we found that the controversy can easily be resolved by taking the numerical finite coordinate range into consideration in constructing the momentum space representation. With this recipe, we have efficiently calculated the photoelectron spectra of hydrogen atom under intense laser pulses [6].

In this paper, we aim to develop a new momentum space CESE (p-CESE) method that preserves the power of CESE and keeps the complete information of the solution simultaneously during time evolution. A Fourier transformation can convert the momentum space solution into coordinate space representation at any time if information in the latter is requested, making the momentum space approach useful for time-dependent systems and scatter-

* Corresponding author at: Institute of Physics, National Chiao-Tung University, Hsinchu 30010, Taiwan.
E-mail address: tfjiang@faculty.nctu.edu.tw (T.F. Jiang).

0010-4655/$ – see front matter
doi:10.1016/j.cpc.2009.10.018

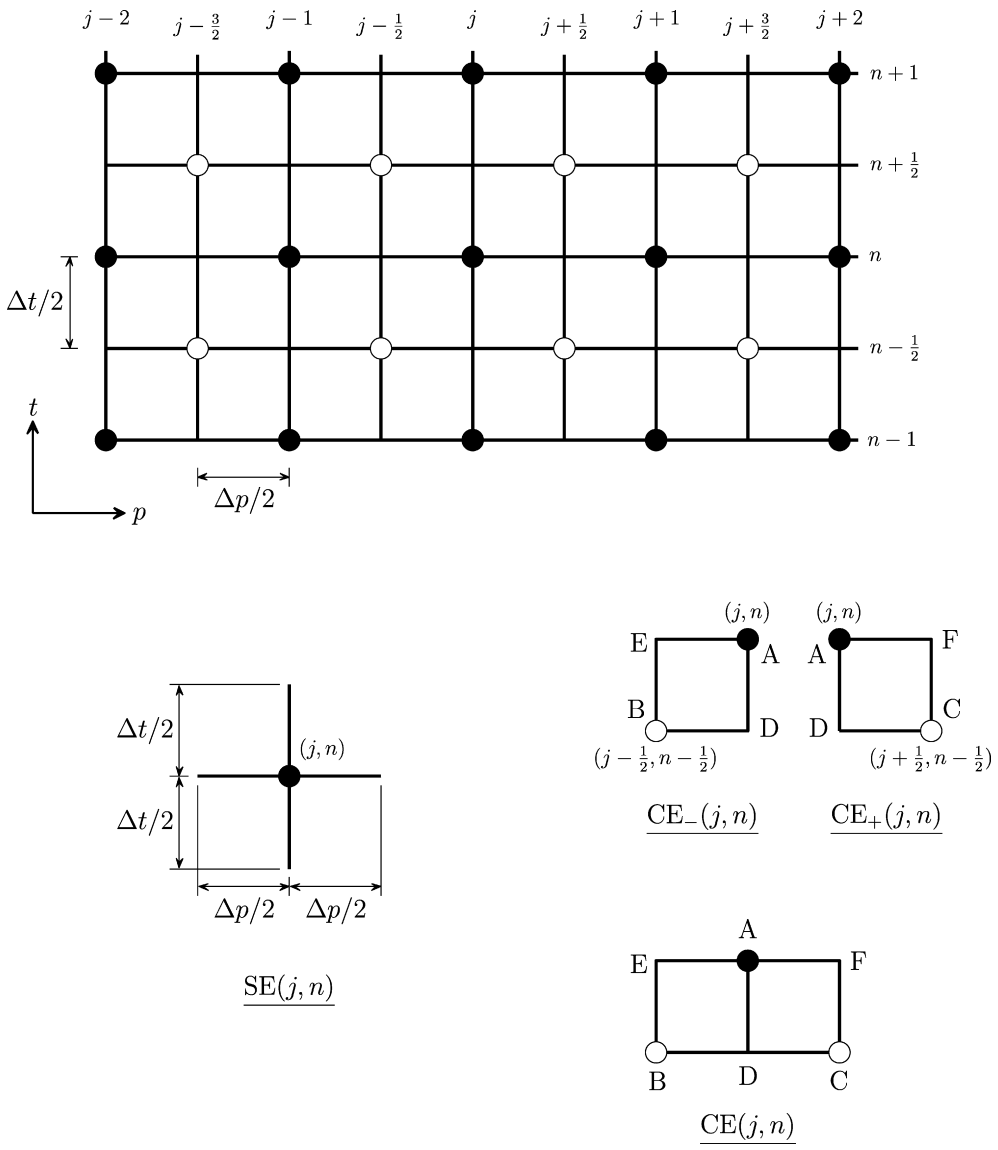

Fig. 1. Definitions of the momentum–time staggered mesh, CE, and SE in E_2.

ing problems. This paper contains the layout of the fundamental ideas of the p-CESE method and justification of this new method by calculating the analytic solutions of some paradigmatic wave equations. The development covered classical, quantum mechanical and nonlinear wave problems. The extension to higher-dimensional systems will be reported in future work. The rest of the paper is organized as follows: In Section 2, we present the formulation of the p-CESE method for the simple wave equation. In Section 3, we treat the convection–diffusion equation. In Section 4, we calculate the time-dependent Schrödinger equation of a driven harmonically oscillating charge. And in Section 5, the nonlinear Korteweg–de Vries (KdV) equation was solved by p-CESE method. Discussion and conclusions are given in Section 6.

2. Simple wave equations and the formulation of momentum space CESE method

Consider first the simple wave equation

$$\frac{\partial u}{\partial t}+a\frac{\partial u}{\partial x}=0, \tag{1}$$

where the wave speed a is a constant. The solution of $u(x,t)$ is in the form of $f(x-at)$ with a shape function f. For positive a, the wave will move toward the positive x direction. Because the numerical range of x is finite, eventually the wave front will reach the numerical boundary in sufficiently long time. The treatment in coordinate space will encounter difficulties if the wave at large distance is important, such as in the scattering state problem. This simple system was employed in Ref. [1] to develop the basic CESE method and was named the a-scheme. Making the following Fourier transformations, the system has the coordinate and the momentum representation alternatively:

$$u(x,t)=\int \tilde{u}(p,t)\,e^{ipx}\,dp,$$
$$\tilde{u}(p,t)=\frac{1}{2\pi}\int u(x,t)\,e^{-ipx}\,dx, \tag{2}$$

the wave equation in momentum representation becomes

$$\frac{\partial \tilde{u}(p,t)}{\partial t}=-iap\tilde{u}(p,t). \tag{3}$$

This is simply an ordinary differential equation. With initial condition $\tilde{u}(p,t=0)$, the solution at any time is

$$\tilde{u}(p,t)=\tilde{u}(p,t=0)\,e^{-ipat}. \tag{4}$$

Obviously, the amplitude of the solution $\tilde{u}(p,t)$ is stationary at any time in the momentum space. Though the equation and its solution in momentum space are rather simple, they serve the development as a calibration example for the p-CESE method. Following the formalism of the a-scheme in coordinate space CESE [1], we derive the a-scheme of p-CESE method below. We define the two-dimensional Euclidean space $(x_1, x_2) \equiv (p,t)$, $\nabla \equiv (\partial/\partial p, \partial/\partial t)$ and the two-dimensional vector $\mathbf{h} \equiv (h_1, h_2) = (0, \tilde{u})$. Then, Eq. (3) becomes

$$\nabla \cdot \mathbf{h} = -ipa\tilde{u}(p,t). \tag{5}$$

The momentum–time (p–t) space is discretized with the staggered SEs and nonoverlapping CEs similarly as described in Ref. [1] except the coordinate x is now the momentum p. For completeness, the p–t space is drawn in Fig. 1. Associated with each $p-t$ mesh point (p_j, t^n), designated as (j,n), is the SE(j,n) shown as the cross line segments passing the mesh point (j,n). Conservation elements CE$_-(j,n)$ and CE$_+(j,n)$ are associated with SE(j,n). Integrating Eq. (5) over the CE$_\pm(j,n)$ and applying the divergence theorem, we have

$$\begin{aligned}
\int_{CE_+} \mathbf{h}\cdot d\mathbf{s} &= \int_{CE_+} \left[-ipa\tilde{u}(p,t)\right] dp\,dt,\\
\int_{CE_-} \mathbf{h}\cdot d\mathbf{s} &= \int_{CE_-} \left[-ipa\tilde{u}(p,t)\right] dp\,dt,
\end{aligned} \tag{6}$$

where $d\mathbf{s}$ is the generalized line element associated with the generalized area element $dp\,dt$, with fixed convention in the normal direction. We take $d\mathbf{s} = (dt, -dp)$, that is, the line integral in each CE is calculated counterclockwise. For the left-hand side of Eqs. (6), the line integrals along t segments are null because $\mathbf{h}\cdot d\mathbf{s} = -\tilde{u}\,dp$, which has no component in the t-direction. For any (p,t) lying on SE(j,n), $\tilde{u}(p,t)$ and $\mathbf{h}(p,t)$ are expanded at $\tilde{u}(p,t;j,n)$ and $\mathbf{h}(p,t;j,n)$ up to the first order, respectively

$$\begin{aligned}
\tilde{u}(p,t;j,n) &\simeq \tilde{u}_j^n + (\tilde{u}_p)_j^n (p-p_j) + (\tilde{u}_t)_j^n \left(t-t^n\right),\\
\mathbf{h}(p,t;j,n) &\simeq \left(0, \tilde{u}(p,t;j,n)\right),
\end{aligned} \tag{7}$$

where (j,n) denotes the mesh point (p_j, t^n). With the expansion, it is seen that on the space–time mesh grids,

$$(\tilde{u}_t)_j^n = -iap_j\tilde{u}_j^n. \tag{8}$$

By Eqs. (7), the flux conservation equations (6) become

$$\tilde{u}_j^n \pm (\tilde{u}_{\bar{p}})_j^n - \left[\tilde{u}_{j\pm\frac{1}{2}}^{n-\frac{1}{2}} \mp (\tilde{u}_{\bar{p}})_{j\pm\frac{1}{2}}^{n-\frac{1}{2}}\right] = -iap_{j\pm\frac{1}{4}}\frac{\Delta t}{2}\tilde{u}_\pm^*, \tag{9}$$

where we designate $\tilde{u}_{\bar{p}} = \frac{\Delta p}{4}\cdot\tilde{u}_p$. $\tilde{u}_\pm^*$ denotes the mean value of $\tilde{u}$ in the integrand of the area integrals of Eqs. (6) such that

$$\int_{CE_\pm} \left[-ipa\tilde{u}(p,t)\right] dp\,dt = -iap_{j\pm\frac{1}{4}}\frac{\Delta t\cdot\Delta p}{4}\tilde{u}_\pm^*, \tag{10}$$

for CE$(j,n)_\pm$, respectively. Since $\tilde{u}_\pm^*$ are not located on our mesh grids, we develop a convenient numerical iteration scheme for time marching. Let the index ℓ indicate the iteration level of convergence. In the first step, $\tilde{u}_\pm^*$ is approximated by $\tilde{u}_{j\pm\frac{1}{4}}^{n-\frac{1}{2}}$; after the initial step, $\tilde{u}_{j\pm\frac{1}{4}}^n$ is employed as the new input $\tilde{u}_\pm^*$. Although these $\tilde{u}_\pm^*$ are not on the mesh grids, they are in the solution elements and Eq. (7) can be used. The iteration scheme goes as follows:

$$\tilde{u}_{j,\ell}^n \pm (\tilde{u}_{\bar{p}})_{j,\ell}^n - \left[\tilde{u}_{j\pm\frac{1}{2}}^{n-\frac{1}{2}} \mp (\tilde{u}_{\bar{p}})_{j\pm\frac{1}{2}}^{n-\frac{1}{2}}\right] = -iap_{j\pm\frac{1}{4}}\frac{\Delta t}{2}\tilde{u}_{\pm,\ell-1}^*. \tag{11}$$

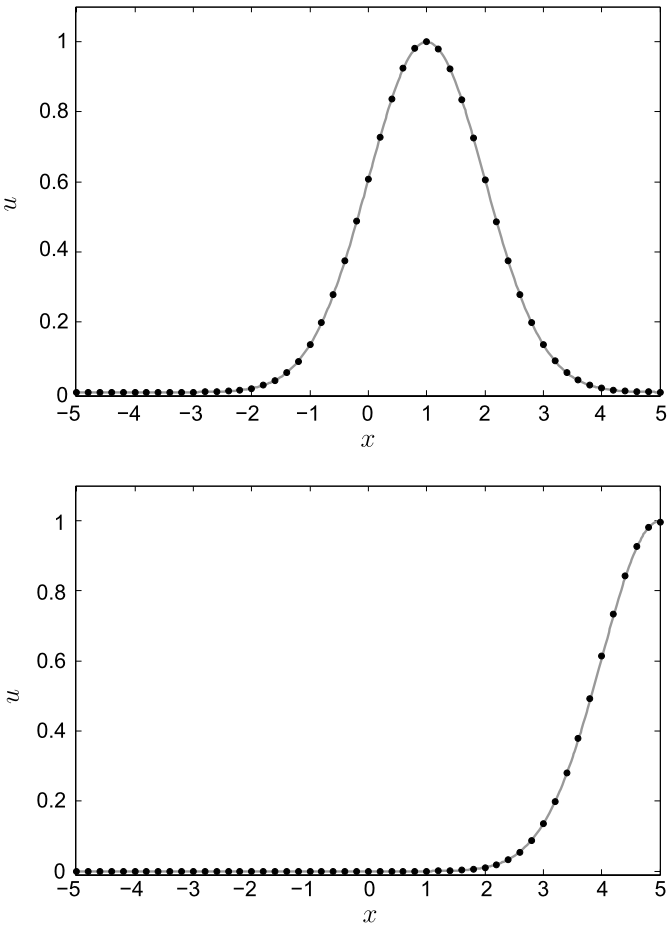

Fig. 2. Results of the coordinate space CESE a-scheme at $t = 1$ and 5 obtained with $x \in [-5, 5]$. Notice that the wave u will flow out the boundary at sufficient long time. Dots: numerical results. Solid line: exact solution.

The iteration is stopped if the convergence criterion

$$\left|\tilde{u}_{j,\ell+1}^n - \tilde{u}_{j,\ell}^n\right| < \varepsilon \tag{12}$$

is satisfied for a plausibly small ϵ, which is usually matched within ten iterations. The time-marching scheme developed above is explicit. From the known $\tilde{u}_{j\pm1/2}^{n-1/2}$ and $(\tilde{u}_{\bar{p}})_{j\pm1/2}^{n-1/2}$ at time level $n-1/2$, we can solve for unknowns $\tilde{u}_j^n$ and $(\tilde{u}_{\bar{p}})_j^n$ at subsequent time level n. A time step Δt consists of two half-time steps $\frac{1}{2}\Delta t$ as in the original CESE method [1].

For testing, we set $a = 1$ and study the following traveling Gaussian wave packet and its Fourier transform:

$$\begin{aligned}
u(x,t) &= e^{-\frac{1}{2}(x-t)^2},\\
\tilde{u}(p,t) &= \frac{1}{\sqrt{2\pi}} e^{-ipt-\frac{p^2}{2}}.
\end{aligned} \tag{13}$$

As a comparison, we perform the coordinate space CESE a-scheme with the range $-5 \leqslant x \leqslant 5$. In Fig. 2 we show the calculated and analytic solutions at $t = 1$ and at $t = 5$. For the case of $t = 1$, the wave is still wholly inside the numerical region; for the case of $t = 5$, part of the wave has already flowed out of the coordinate space. The NRBC derived from flux conservation automatically gives a smooth leakage of wave through the numerical boundary without causing aliased reflection error.

Next we calculate the same wave equation through the developed a-scheme of the p-CESE method using $\Delta p = 0.16$, $\Delta t = 0.08$ and the Courant number 0.5. Fig. 3 shows the real part and the imaginary part of the analytic and computed waves at $t = 5$. Note

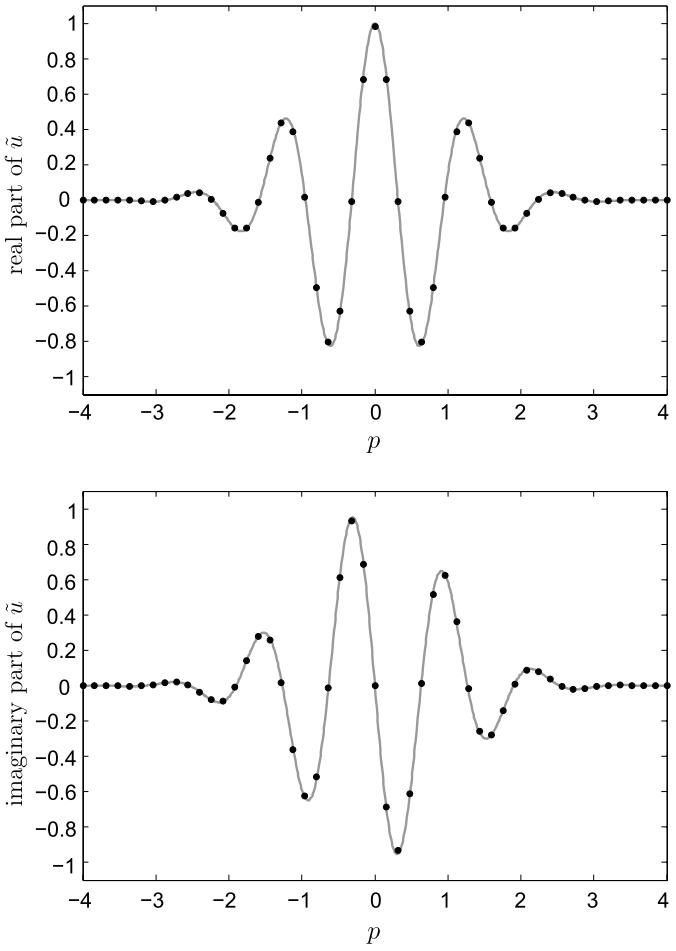

Fig. 3. Computational results $\tilde{u}$ at $t = 5$ by the p-CESE method. Data obtained with $p \in [-5, 5]$, $\Delta p = 0.16$, and $\Delta t = 0.08$. Dots: numerical results. Solid line: exact solution.

that $|\tilde{u}(p,t)| = e^{-\frac{p^2}{2}}$, thus the momentum space solution at the boundary is equal to $e^{-12.5} = 3.7 \times 10^{-6}$ times of its peak value at $p = 0$, appropriate to be considered as vanishing. Therefore we can take the momentum space wave as stationary with no flow out of the numerical region. The behavior of computational errors will be discussed in the section of KdV equation later, but basically the error is visually invisible. The results of this section imply that for a traveling wave, the momentum space method contains more complete information than the coordinate space method, and the formulation of the new p-CESE method is justified.

3. Convection–diffusion equations

Next, we consider the convection–diffusion equation:

$$\frac{\partial u}{\partial t} + a\frac{\partial u}{\partial x} - \mu\frac{\partial^2 u}{\partial x^2} = 0, \tag{14}$$

where the wave velocity a, and the viscosity coefficient μ are constants, called the μ-scheme in the CESE framework [1]. By Fourier transformation, Eq. (14) can be transformed into the momentum space form,

$$\frac{\partial \tilde{u}}{\partial t} + \big(iap + \mu p^2\big)\tilde{u} = 0. \tag{15}$$

Applying the Gauss divergence theorem to the two-dimensional p–t space,

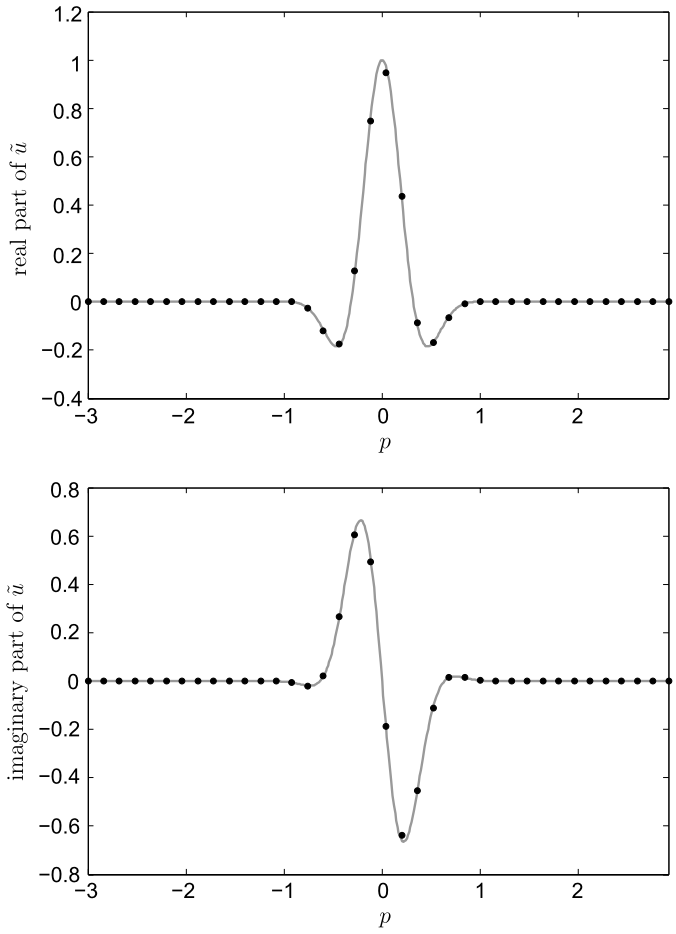

Fig. 4. Results of $\tilde{u}$ at $t = 5$ obtained with $p \in [-5, 5]$ at $\Delta p = 0.16$, and $\Delta t = 0.16$. Dots: numerical results. Solid line: exact solution.

$$\oint_{S(\mathrm{CE}_\pm(j,n))} \mathbf{h}\cdot d\mathbf{s} = -\int_{\mathrm{CE}_\pm(j,n)} \big(iap + \mu p^2\big)\tilde{u}\,dp\,dt, \tag{16}$$

where $\mathbf{h} \equiv (h_1, h_2) = (0, \tilde{u})$, we can see that with $\tilde{u} = \tilde{u}(p, t; j, n)$ defined by Eq. (7), at the mesh points (j, n),

$$(\tilde{u}_t)_j^n = -\big(iap_j + \mu p_j^2\big)\tilde{u}_j^n. \tag{17}$$

The explicit time-marching scheme is derived similarly to the previous simple wave case, that is,

$$\tilde{u}_{j,\ell}^n \pm (\tilde{u}_{\bar{p}})_{j,\ell}^n - \big[\tilde{u}_{j\pm\frac{1}{2}}^{n-\frac{1}{2}} \mp (\tilde{u}_{\bar{p}})_{j\pm\frac{1}{2}}^{n-\frac{1}{2}}\big] = -\frac{\Delta t}{2}\big(iap_{j\pm\frac{1}{4}} + \mu p^2_{j\pm\frac{1}{4}}\big)\tilde{u}^*_{\pm,\ell-1}, \tag{18}$$

where ℓ is the iteration index and the iterative scheme is the same as described in the previous section. With the aid of Eqs. (17) and (18), the unknowns $\tilde{u}_j^n$ and $(\tilde{u}_{\bar{p}})_j^n$ can be solved iteratively in terms of known $\tilde{u}_{j\pm1/2}^{n-1/2}$ and $(\tilde{u}_{\bar{p}})_{j\pm1/2}^{n-1/2}$ in the preceding time level.

The momentum space convection–diffusion equation is also an ordinary differential equation with the general solution

$$\tilde{u}_e(p,t) = f(p) \times \exp\big[-\big(iap + \mu p^2\big)t\big], \tag{19}$$

with an arbitrary shape function $f(p)$. As a calibration of the p-CESE method, we use a Gaussian shape $f(p) = \exp(-p^2)$ below. The numerical results for $a = 1$ and $\mu = 1$ at $t = 5$ are depicted in Fig. 4, showing excellent agreements between calculated and exact solutions. As we know, solving Eq. (14) in coordinate space is not

as straightforward as this momentum space approach. A c-scheme with numerical dissipation was implemented for the treatment in the coordinate space approach [2], while the simplest a-scheme in p-CESE method already gives accurate results. For a reference, the exact solution in coordinate space corresponds to Eq. (19) is

$$u(x,t)=\sqrt{\frac{\pi}{1+\mu t}}\times\exp\left[\frac{-(x-at)}{4(1+\mu t)}\right]. \tag{20}$$

4. Driven simple harmonic oscillator

Next we solve a quantum mechanical problem by the p-CESE method. Under the velocity gauge and the dipole approximation, a charge q oscillating in the simple harmonic potential with applied electromagnetic pulse is described by the time-dependent Schrödinger equation

$$i\frac{\partial u}{\partial t}=\left[\frac{p^2}{2}+\frac{1}{2}\Omega^2x^2-A(t)\cdot p\right]u. \tag{21}$$

Throughout this section, we use atomic units $\hbar=1$, $m=1$ and $e=1$, thus 1 a.u. laser peak intensity equals to 7.02×10^{16} W/cm^2. The relationship between electric field and vector potential is given by

$$E(t)=-\partial A(t)/\partial t.$$

The transition probability from the ground state $|0>$ to an excited state $|N>$ is given by Poisson's distribution [7]

$$P_{0\to N}=e^{-\sigma}\frac{\sigma^N}{N!}, \tag{22}$$

where σ is a pulse parameter

$$\sigma=\frac{1}{2\Omega}\left|\int_{\infty}^{\infty}E(t)e^{i\Omega t}\,dt\right|^2. \tag{23}$$

Recast Eq. (21) into p-space, we obtain

$$i\tilde{u}_t+\frac{1}{2}\Omega^2\tilde{u}_{pp}=\left[\frac{p^2}{2}-A(t)\cdot p\right]\tilde{u}. \tag{24}$$

With $\tilde{u}=\tilde{u}(p,t;j,n)$ and expansion of Eq. (7) at mesh point (j,n), Eq. (24) becomes

$$(\tilde{u}_t)_j^n=-i\left[\frac{p_j^2}{2}-A\left(t^n\right)\cdot p_j\right]\tilde{u}_j^n. \tag{25}$$

Furthermore, for $(p,t)\in \mathrm{SE}(j,n)$, we define

$$\mathbf{h}(p,t;j,n)=\left(\frac{1}{2}\Omega^2\tilde{u}_p(p,t;j,n),i\tilde{u}(p,t;j,n)\right), \tag{26}$$

and the flux theorem for $\mathrm{CE}_{\pm}(j,n)$ becomes

$$\oint_{S(\mathrm{CE}_{\pm}(j,n))}\mathbf{h}\cdot d\mathbf{s}=\int_{\mathrm{CE}_{\pm}(j,n)}\left[\frac{p^2}{2}-A(t)\cdot p\right]\tilde{u}\,dp\,dt. \tag{27}$$

Evaluating the area integral over $\mathrm{CE}_{\pm}(j,n)$ by the mean value method of $\tilde{u}_{\pm}^*$ as described in former sections, we obtain

$$\begin{aligned}&i\left\{\tilde{u}_{j,\ell}^n\pm(\tilde{u}_{\bar{p}})_{j,\ell}^n-\left[\tilde{u}_{j\pm\frac{1}{2}}^{n-\frac{1}{2}}\mp(\tilde{u}_{\bar{p}})_{j\pm\frac{1}{2}}^{n-\frac{1}{2}}\right]\right\}\\&\quad\mp\frac{1}{2}\Omega^2\frac{\Delta t}{\Delta p}\left[(\tilde{u}_p)_{j,\ell}^n-(\tilde{u}_p)_{j+\frac{1}{2}}^{n-\frac{1}{2}}\right]\\&=\frac{\Delta t}{2}\left[\frac{p_{j\pm\frac{1}{4}}^2}{2}-A\left(t^{n-\frac{1}{4}}\right)\cdot p_{j\pm\frac{1}{4}}\right]\times\tilde{u}_{\pm}^*,\end{aligned} \tag{28}$$

where ℓ is the iteration index, and the iteration scheme as in previous sections is applied for time marching. With the aid of Eqs. (25) and (28), the unknowns $\tilde{u}_j^n$ and $(\tilde{u}_{\bar{p}})_j^n$ can be solved iteratively in terms of the known $\tilde{u}_{j\pm1/2}^{n-1/2}$ and $(\tilde{u}_{\bar{p}})_{j\pm1/2}^{n-1/2}$ of the previous time level. As an illustration of the method, we choose a light pulse with a $\sin^2$ envelop,

$$\begin{aligned}&E(t)=E_m\sin^2\frac{\pi t}{T}\cos\omega t,\\&0<t<T.\end{aligned} \tag{29}$$

We assume the carrier frequency of the electric field is $\omega=0.057$ a.u. (800 nm in wavelength), $E_m=0.002$ a.u., and the total time duration T is 8 optical cycles. Furthermore, we assume the near resonant case, $\Omega=0.058$ so that excitations are significant. The system is initially prepared in the ground state

$$\tilde{u}(p,t=0)=\frac{1}{(\Omega\pi)^{\frac{1}{4}}}\exp\left(-\frac{p^2}{2\Omega}\right). \tag{30}$$

The transition probabilities $P_{0\to N}$ from the ground state to other excited state N are listed in Table 1, calculated from the overlap of the final wave function $\tilde{u}(p,t=T)$ with the eigenstate $\tilde{u}_N$:

$$P_{0\to N}=\left|\int_{-\infty}^{\infty}\tilde{u}\tilde{u}_N^*\,dp\right|^2. \tag{31}$$

We can see that reasonably good results are obtained through the p-CESE method, and the error in each transition probability is scaled nearly to $(\Delta p)^2$ with different grids. This error behavior will be discussed in KdV system.

5. The Korteweg–de Vries equation

The *Korteweg–de Vries* (KdV) equation is a classic example of the nonlinear wave equations [8,9]. The general form is

$$\frac{1}{\beta}\frac{\partial u}{\partial t}+\frac{\alpha}{\gamma}u\frac{\partial u}{\partial x}+\frac{1}{\gamma^3}\frac{\partial^3u}{\partial x^3}=0, \tag{32}$$

where α, β and γ are nonzero constants. The system contains both nonlinearity and dispersion. For convenience, we study in this section the scaled equation

$$u_t-6uu_x+u_{xxx}=0. \tag{33}$$

By Fourier transformation and some manipulations, the momentum space equation is

$$\tilde{u}(p,t)_t=3ip\int_{-\infty}^{\infty}\tilde{u}(q,t)\tilde{u}(p-q,t)\,dq+ip^3\tilde{u}. \tag{34}$$

Let $\mathbf{h}=(0,\tilde{u})$ and applying the Gauss divergence theorem in E_2, Eq. (34) becomes

$$\oint_{S(V)}\mathbf{h}\cdot d\mathbf{s}=\int_V\left[3ip\int_{-\infty}^{\infty}\tilde{u}(q,t)\tilde{u}(p-q,t)\,dq+ip^3\tilde{u}\right]dp\,dt. \tag{35}$$

We can see that for a nonlinear system, the source terms on the right-hand side of Eq. (34) contain the convolutional integral of unknown functions, hence the straightforward explicit iteration scheme described in previous sections does not work. We implement two new ideas for the treatment of nonlinear problems in the p-CESE method. First, at each time level, we calculate $\tilde{u}(p,t)$ and $\tilde{u}_p(p,t)$ at grids of half spacings, instead of spacings at staggered Δp in linear examples. The convolutional integral can

Table 1
Numerical results of transition probability from the ground state to state $|N\rangle$. Also listed are the exact values and the errors. Three grid spacings $\Delta p = 0.08, 0.04$ and 0.02 were used in calculations. The time step $\Delta t = 8 \times 10^{-4}$ is used throughout.

N	$P_{0\to N}$						
	Exact	$[\Delta p = 0.02$	Error]	$[\Delta p = 0.04$	Error]	$[\Delta p = 0.08$	Error]
0	0.1951894	0.1948923	−2.97(−4)	0.1940719	−1.12(−3)	0.1916537	−3.54(−3)
1	0.3188975	0.3183566	−5.41(−4)	0.3168929	−2.00(−3)	0.3130507	−5.85(−3)
2	0.2605050	0.2603970	−1.08(−4)	0.2602243	−2.81(−4)	0.2612223	7.17(−4)
3	0.1418697	0.1421716	3.02(−4)	0.1430856	1.21(−3)	0.1462422	4.37(−3)
4	0.0579461	0.0582811	3.35(−4)	0.0591675	1.22(−3)	0.0609044	2.96(−3)
5	0.0189343	0.0191296	1.95(−4)	0.0195836	6.49(−4)	0.0198997	9.65(−4)
6	0.0051558	0.0052353	7.95(−5)	0.0053896	2.34(−4)	0.0053358	1.80(−4)
7	0.0012033	0.0012287	2.54(−5)	0.0012640	6.07(−5)	0.0012595	5.62(−5)
$\sum P_{0\to N} =$	0.9997011	0.9996922		0.9996794		0.9995683	

Note: $-2.97(-4)$ denotes -2.97×10^{-4}.

then be calculated by Simpson's rule [10]. Second, for every half-marching time step, say from $t^{n-\frac{1}{2}}$ to t^n, we begin by using $\tilde{u}$ and $\tilde{u}_p$ at $t^{n-\frac{1}{2}}$ for the source terms and find the solution at t^n, then with the obtained, we can find $\tilde{u}$ and $\tilde{u}_p$ at grids $(j \pm \frac{1}{4}, n)$ through the expansion with respect to $\mathrm{SE}(j,n)$ as in Eqs. (7). These are used in the source terms to generate new solutions iteratively until the convergent criterion is satisfied. Usually the results converge within a few iterations.

In mathematical forms, from the conservation laws for $\mathrm{CE}_{\pm}(j,n)$,

$$\oint_{S(\mathrm{CE}_{\pm}(j,n))} \mathbf{h}(x,t;j,n)\cdot d\mathbf{s} = 3ip \int_{\mathrm{CE}_{\pm}(j,n)} \left(\int_{-\infty}^{\infty} \tilde{u}(q,t)\tilde{u}(p-q,t)\,dq \right) dp\,dt + \int_{\mathrm{CE}_{\pm}(j,n)} ip^3 \tilde{u}\,dp\,dt, \tag{36}$$

where $\mathbf{h}(p,t;j,n) = (0, \tilde{u}(p,t;j,n))$. We can derive the following a-scheme iterations

$$u_j^n = \frac{1}{2}\left\{ [u - u_{\bar{p}}]_{j+\frac{1}{2}}^{n-\frac{1}{2}} + [u + u_{\bar{p}}]_{j-\frac{1}{2}}^{n-\frac{1}{2}} \right\} + \frac{F}{\Delta p} + \frac{G}{\Delta p},$$
$$u_{\bar{p}},_j^n = \frac{1}{2}\left\{ [u - u_{\bar{p}}]_{j+\frac{1}{2}}^{n-\frac{1}{2}} - [u + u_{\bar{p}}]_{j-\frac{1}{2}}^{n-\frac{1}{2}} \right\} + \frac{F}{\Delta p} - \frac{G}{\Delta p}, \tag{37}$$

where we designate $u_j^n = \tilde{u}(p_j, t^n)$, $u_{\bar{p}},_j^n \equiv \frac{\Delta p}{4}(\tilde{u}_p)_j^n$, and $\Delta\tau = \frac{\Delta p}{2}\frac{\Delta t}{2}$ for shorthand. And

$$F = \left\{ 3ip_{i+1/2} \sum_j u\left(p_{i+1/2} - q_j, t^{n-1/2}\right) u\left(q_j, t^{n-1/2}\right) \frac{\Delta p}{2} + ip_{i+1/2}^3 u\left(p_{i+1/2}, t^{n-1/2}\right) \right\} \Delta\tau,$$

$$G = \left\{ 3ip_{i-1/2} \sum_j u\left(p_{i-1/2} - q_j, t^{n-1/2}\right) u\left(q_j, t^{n-1/2}\right) \frac{\Delta p}{2} + ip_{i-1/2}^3 u\left(p_{i-1/2}, t^{n-1/2}\right) \right\} \Delta\tau.$$

The KdV equation (33) has a solitonic solution

$$u(x,t) = -\frac{c}{2}\,\mathrm{sech}^2\left(\frac{\sqrt{c}}{2}(x - ct + x_0) \right). \tag{38}$$

Note that the solution depends on the speed c of soliton and therefore multiplying the solution by an arbitrary constant is no longer a solution. Without loss of generality, we set the initial peak position at $x_0 = 0$ with the wave propagating at speed c to the right of the x-axis without shape change. The exact solution in momentum space is

$$\tilde{u}_e(p,t) = -p\,\mathrm{csch}\left(\frac{\pi p}{\sqrt{c}} \right) \exp(-ipct). \tag{39}$$

Figs. 5a and 5b depict the real and the imaginary part of the numerical results together with the analytic results at time $t = 5$ and show excellent agreements between the p-CESE calculation and the analytic results.

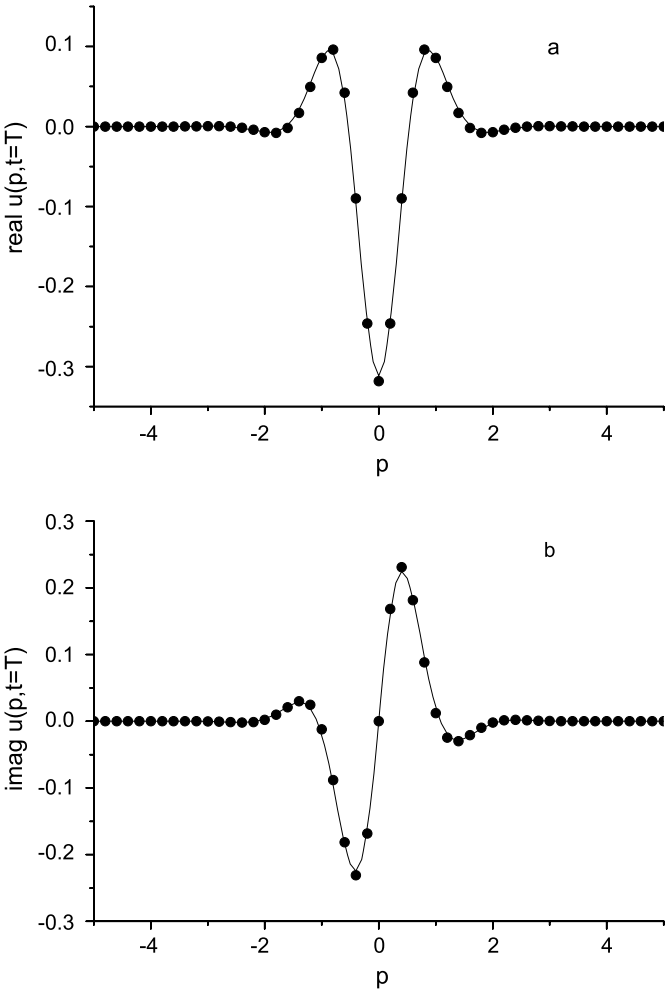

Fig. 5. Results of the real and imaginary part of KdV solution at $t = 5$ obtained with $p \in [-5, 5]$ and $\Delta t = 0.01$. Solid line: analytical solution, dots: numerical results.

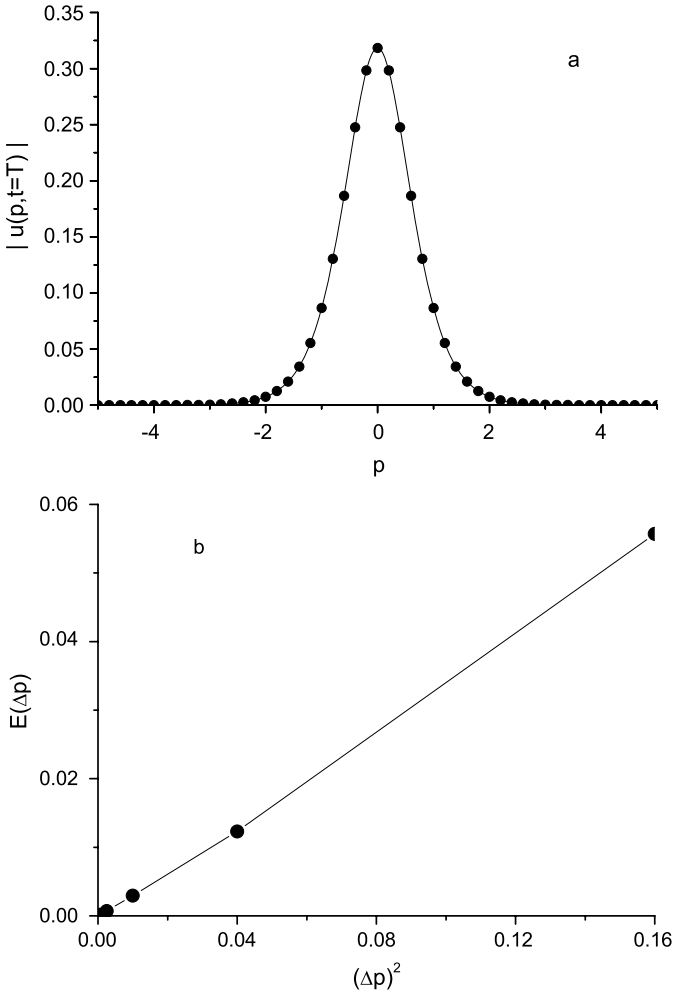

Fig. 6. (a) Results of the magnitude of KdV solution at $t = 5$ obtained with $p \in [-5, 5]$ and $\Delta t = 0.01$. Solid line: exact solution, dots: numerical results. (b) Error as function of square of grid size Δp. It shows $\sim O(\Delta p)^2$ behavior.

In Fig. 6a, comparison of the magnitudes of the calculated and the exact solutions at $t = 5$ with $c = 1$ is shown. For the soliton solution, although the real part and the imaginary part oscillate with time, the magnitude is stationary as seen from Eq. (39).

The previous section has shown that our developed p-CESE method works well for various kinds of wave problems. Here we present the error analysis for this method. We define the root-mean-square error at the final moment of time as follows:

$$E(N) = \sqrt{\frac{1}{N}\sum_{j=0}^{j=N}\left[u\left(p_j, t^{final}\right) - u_{exact}\right]^2}. \tag{40}$$

In Table 2, we listed the errors with respect to the grid size Δp and in Fig. 6b the error versus $(\Delta p)^2$ are plotted. The straight line shows that the error behaves as $\sim O(\Delta p)^2$, a general scaling behavior of our developed p-CESE a-scheme method.

6. Discussion and conclusions

In this paper, we developed the CESE method in momentum space on a fundamental scope and explored the solutions of several paradigmatic wave equations, namely the basic one-dimensional wave equation, the convection–diffusion equation, the driven quantum mechanical problem and the nonlinear KdV equation. In each problem, we developed an explicit time-marching scheme in the p-CESE method. While it is straightforward for linear problems, for nonlinear problems such as the KdV equation, convolution integral of unknown functions in the source term is involved. This difficulty is resolved by employing the half-step grid size for the convolutions and the iterations during time marching. Each system was calibrated with a known exact solution, and we showed that the p-space CESE method works well for systems from classical wave equations, quantum mechanical problems to nonlinear equations, and the error behavior of the developed scheme is $\sim O(\Delta p)^2$. The main advantages of the p-CESE method, in cooperation with the superior CESE method in coordinate space, are threefold. *First*, like the original CESE method, applying the momentum–time flux conservation concept in staggered mesh, the explicit time marching scheme for every wave equation can be derived. *Second*, the boundary conditions are fulfilled automatically. That is, for a sufficient large momentum value, the wave and its derivatives are simply vanishing small at the numerical boundary, because the kinetic energy of a system is physically finite. *Third*, the information of the wave is completely preserved within the numerical momentum region, without loss at the boundary as in the coordinate space method. This will be especially useful in treating scattering problems. In this paper, we aim to develop a method for waves that extend to far distance as time goes on. This category of problems is closely related to the experimental problems such as photoelectron spectra, etc. The problem with waves extending to far distances is not easy to treat by coordinate space methods, as demonstrated in Fig. 2. We show that the p-CESE is capable for this kind of problem. On the other hand, the boundary value problems in finite domain were solved neatly by coordinate space CESE method [1], and is not our goal here. Our algorithm follows the core scheme of CESE method, and the stability criterion has been rigorously discussed [1,11]. The criterion in our scheme is $a\,dt/dp \leqslant 1$. Also, in each time step, we calculate the correlation integral and the cost is $\sim O(N^2)$ for N grid points. During each time step, there is an iteration scheme for accurate computation of the correlation integral. However, the integral converges within ten iterations, so the cost is $\sim c \cdot O(N^2)$ where c is a constant of order 1. The computational cost can be compared with other conventional finite-difference schemes. Finally, for realistic problems, higher-dimensional method is necessary. This problem, together with higher order of accuracy p-CESE method, is currently under development.

Table 2
The root-mean-square error $E[N]$ versus mesh size Δp shows $O(\Delta p^2)$ behavior for KdV equation in our p-CESE method under the a-scheme.

N	Δp	$E[N]$
26	0.4	5.57×10^{-2}
51	0.2	1.23×10^{-2}
101	0.1	2.94×10^{-3}
201	0.05	7.18×10^{-4}
401	0.025	1.72×10^{-4}
801	0.0125	3.57×10^{-5}

Acknowledgements

T.F.J. thanks the support of NSC, Taiwan under the contract of number NSC97-2112-M-009-002-MY3. He also acknowledges the hospitality of NASA/NIA through the MoE between NASA and NARL, Taiwan.

References

[1] S.C. Chang, W.M. To, A new numerical framework for solving conservation laws — The method of space–time conservation element and solution element, NASA/TM 104495, 1991;
S.C. Chang, J. Comput. Phys. 119 (1995) 295.

[2] More details and references can be found in http://www.grc.nasa.gov/WWW/microbus/.
[3] S.-C. Chang, A. Himansu, C.-Y. Loh, X.-Y. Wang, S.-T.J. Yu, Robust and simple non-reflecting boundary conditions for the Euler equations, A new approach based on the space–time CE/SE method, NASA/TMX2003-212495/REV1, 2003.
[4] See, for example, Tsin-Fu Jiang, Shih-I Chu, Phys. Rev. A 46 (1992) 7322.
[5] U.L. Pen, T.F. Jiang, Phys. Rev. A 46 (1992) 4297;
U.L. Pen, T.F. Jiang, Phys. Rev. A 53 (1996) 623.
[6] See T.F. Jiang, Comput. Phys. Commun. 178 (2008) 571, and references therein.
[7] C. Cohen-Tannoudji, J. Dupont-Roc, C. Fabre, G. Grynberg, Phys. Rev. A 8 (1973) 2747.
[8] P.G. Drazin, R.S. Johnson, Solitons: An Introduction, Cambridge Univ. Press, Cambridge, 1989.
[9] G.B. Arfken, H.J. Weber, Mathematical Methods for Physicists, 4th ed., Academic Press, San Diego, 1995, Section 8.1.
[10] J.H. Mathews, K.D. Fink, Numerical Methods Using Matlab, 4th ed., Pearson Prentice Hall, London, 2004, Section 7.2.
[11] Sin-Chung Chang, On space–time inversion invariance and its relation to non-dissipatedness of a CESE core scheme, AIAA paper 2006-4779, 2006.